Ferrofluids from Magnetic−Chitosan Hybrids

V. Belessi,[†,‡] R. Zboril,[§] J. Tucek,[§] M. Mashlan,[§] V. Tzitzios,[†] and D. Petridis*[,†]

Institute of Materials Science, NCSR "Demokritos", Agia Paraskevi 15310 Athens, Greece, Department of Food Technology, Technological Educational Institution of Athens, Agiou Spyridonos Street, 122 10 Egaleo, Athens, Greece, and Department of Physical Chemistry and Nanomaterials Research Centre, Palacky University, Svobody 26, 77146 Olomouc, Czech Republic

Received October 17, 2007. Revised Manuscript Received February 5, 2008

Magnetic nanoparticles coated with chitosan or quaternized chitosan were synthesized by a new route and characterized by X-ray diffraction (XRD), transmission electron microscopy (TEM), temperature dependent and in-field Mössbauer spectroscopy, FTIR, thermal analysis (TG/DTA), zeta potential, and magnetic measurements. The prepared ferrofluids were stable for a relatively long time. Mössbauer spectra recorded in an external magnetic field of 5 T establish the formation of "nonstoichiometric magnetite" exhibiting the perfect ferrimagnetic ordering with a low degree of spin canting and frustration. Magnetic measurements confirm the desired properties of the magnetic chitosan for biomedical applications including the superparamagnetic character at room temperature and a high saturation magnetization achievable at low applied fields. The successful and full capping of particles is indicated mainly from magnetic and DTA data through the suppressed interparticle interactions and a significant shift in the transformation temperature of the magnetic cores to hematite. The core−shell structure is definitely proved by TEM observations showing the well crystalline cubic particles with the log-normal size distribution between 10 and 40 nm, which are fully coated with narrow shell of the chitosan matrix.

Introduction

An ever increasing interest in the synthesis, characterization, and surface modification of magnetic nanoparticles has been stimulated by their use in well recognized biomedical and biotechnological applications including targeted drug delivery, magnetic cell separation, enzyme immobilization, magnetic resonance imaging (MRI), and hyperthermia treatments.[1–13] In such applications, magnetite (Fe_3O_4) and maghemite (γ-Fe_2O_3) possess an outstanding position because they are nontoxic, biocompatible, and often present at high levels of accumulation in the target issue or organ.

For biomedical applications, the magnetite nanoparticles should reveal a high saturation magnetization at room temperature. In this way, they can be controlled by an external magnetic field and, thus, concentrated at a targeted area. When magnetic nanoparticles are delivered through the blood stream, their agglomeration is strictly prohibited because it can cause death by emboli. To avoid agglomeration, and at the same time, endow the nanoparticles with other desirable properties, such as water dispersibility, stability, drug, and protein loading capacity, they are subjected to surface modification. Usually, aqueous dispersion of the magnetic nanoparticles is attained by coating their surfaces with hydrophilic polymers, such as starch or dextran, and then the therapeutic agent of interest is either chemically conjugated or ionically bound to the outer layer of the polymer.[14–17]

In this work, we have exploited the use of chitosan as an effective stabilizing agent for magnetic iron oxide nanoparticles. A chitosan coating is expected to prevent aggregation of magnetic particles, to secure their dispersion to aqueous media and also to functionalize the magnetite surfaces so that they can bind drugs, proteins, enzymes, or other biological entities and making such complexes highly suitable for biomedical applications.

* To whom all correspondence should be addressed. E-mail: dpetrid@ims.demokritos.gr. Tel.: 00302106503343. Fax: 00302106519430.
† Institute of Materials Science, NCSR "Demokritos".
‡ Technological Educational Institution of Athens.
§ Palacky University.

(1) Safarik, I.; Safarikova, M. *J. Chromatogr. B.* **1999**, *722*, 33.
(2) Safarik, I.; Safarikova, M. *Biol. Magn. Res. Technol.* **2004**, *2*, 7.
(3) Ito, A.; Shinkai, M.; Honda, H.; Kobayashi, T. *J. Biosci. Bioeng.* **2005**, *100*, 1.
(4) Shinkai, M. *J. Biosci. Bioeng.* **2002**, *94*, 606.
(5) Jordan, A.; Scholz, R.; Wust, P.; Fahling, H.; Felix, R. *J. Magn. Magn. Mater.* **1999**, *201*, 413.
(6) Kim, D. K.; Zhang, Y.; Kehr, J.; Klason, T.; Bjelke, B.; Muhammed, M. *J. Magn. Magn. Mater.* **2001**, *225*, 256.
(7) Fu, L.; Dravid, V. P.; Johnson, D. L. *Appl. Surf. Sci.* **2001**, *181*, 173.
(8) Kim, E. H.; Lee, H. S.; Kwak, B. K.; Kim, B. K. *J. Magn. Magn. Mater.* **2005**, 289–328.
(9) Hilger, I.; Hergt, R.; Kaiser, W. A. *J. Magn. Magn. Mater.* **2005**, *293*, 314.
(10) Neuberger, T.; Schöpf, B.; Hofmann, H.; Hofmann, M.; von Rechenberg, B. *J. Magn. Magn. Mater.* **2005**, *293*, 483.
(11) Pankhurst, Q. A.; Connoly, J.; Jones, S. K.; Dobson, J. *J. Phys. D: Appl. Phys.* **2003**, *36*, R167.
(12) Ma, Z.; Guan, Y.; Liu, X.; Liu, H. *Polym. Adv. Technol.* **2005**, *16*, 554.
(13) Jain, T. K.; Morales, M. A.; Sahoo, S. K.; Leslie-Pelecky, D. L.; Labhasetwar, V. *Mol. Pharm.* **2005**, *2*, 194.
(14) Bergemann, C.; Muller-Schulte, D.; Oster, J,à; Brassard, L.; Lubbe, A. S *J. Magn. Magn. Mater.* **1999**, *194*, 45.
(15) Alexiou, C.; Arnold, W.; Klein, R. J.; Parak, F. G.; Hulin, P.; Bergemann, C.; Erhardt, W.; Wagenpfeil, S.; Lubbe, A S *Cancer Res.* **2000**, *60*, 6641.
(16) Mehta, R. V.; Upadhyay, R. V.; Charles, S. W.; Ramchand, C. N. *Biotechnol. Tech.* **1997**, *11*, 493.
(17) Koneracka, M.; Kopcansky, P.; Timko, M.; Ramchand, C. N.; de Sequeira, A.; Trevan, M. *J. Mol. Catal. B: Enzym.* **2002**, *18*, 13.

10.1021/cm702990t CCC: $40.75
Published on Web 04/24/2008

Scheme 1. Chemical Structure of Chitosan

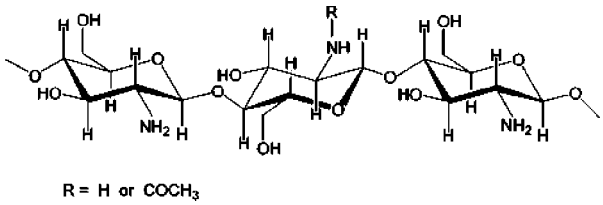

Chitosan (see Scheme 1) is a biocompatible, biodegradable, bioactive, and nontoxic polymer derived from the partial deacetylation of chitin. In fact, chitosan describes a series of polymers with different degrees of deacetylation and different molecular weights (from 50 to 2000 kDa).[18] These two factors determine its physicochemical properties, while the presence of free amine groups provides solubility and, furthermore, it can bind proteins, enzymes and other biomolecules to its frame through chemical reactions.[19–28] Chitosan has been proposed to be an ideal support material for enzyme immobilization because of its improved mechanical strength, resistance to chemical degradation, antibacterial action etc.[24–28]

A main disadvantage of chitosan arises from its weak basic properties that render the macromolecule soluble only in acidic solutions at pH values below 6.0. At neutral pH values, chitosan molecules loose their charge and precipitate from solution. This interferes with the biomedical application of the polymer, especially, at the physiological pH value of 7.4 where chitosan is insoluble and thus less effective. To overcome this obstacle, the synthesis of quaternized *N*-trimethyl chitosan chloride (NQC), exhibiting improved aqueous solubility and antibacterial activity, has been reported.[29–32] More specifically, the quaternized structure of chitosan (see Scheme 2) prevents intermolecular hydrogen bonding between the amine and hydroxylic groups resulting in improved solubility.[33]

Additionally, it has been shown that the quaternized structure possesses antibacterial activity, which increases with increasing the chain length of the alkyl substituent.[32] In vitro

Scheme 2. Chemical Structure of Quaternized *N*-Trimethyl Chitosan

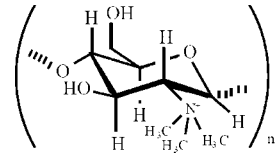

studies have reported that these NQC derivatives enhance the transport of small hydrophilic compounds, e.g., mannitol, and also improve the transport of large drug molecules, such as buserelin, insulin, and octreotide acetate.[34–39] It is generally agreed that the promoting effect of the NQC derivatives increases with increasing the degree of quaternization.[34–38]

Magnetic chitosan composites have been reported in the literature.[28,40–47] Most of the studies describe the encapsulation of the magnetic iron oxide into chitosan microspheres. The present study describes the direct coating of magnetite surfaces with chitosan or quaternized chitosan derivatives. Such magnetic chitosan derivatives offer the possibility to obtain biocompatible magnetic chitosan formulations with improved aqueous dispersibility, stability, and enhanced antibacterial and permeation properties for biomedical applications.

Experimental Section

Materials. All the reactants and solvents were of analytical grade. Chitosan with medium molecular weight was obtained from Fluka. Ammonium peroxydisulfate $(NH_4)_2S_2O_8$, ammonium iron (II) sulfate hexahydrate $Fe(NH_4)_2(SO_4)_26H_2O$, and potassium hydroxide KOH were obtained from Aldrich and used as received.

Preparation of Magnetite. A solution of 2 g of $Fe(NH_4)_2(SO_4)_26H_2O$ in 50 mL of distilled water was mixed with a solution of 1.14 g KOH in 20 mL of H_2O. Subsequently, 0.38 g of $(NH_4)_2S_2O_8$ was added into the reaction system. The mixture was homogenized with magnetic stirring and the reaction was kept at 60 °C for 1 h. After cooling to room temperature the magnetite solid was separated from the solution by centrifugation (1000 rpm/5

(18) Illum, L. *Pharm. Res.* **1998**, *15*, 1326.
(19) Senel, S.; Kremer, M. J.; Kas, S.; Wertz, P. W.; Hincal, A. A.; Squier, C. A *Biomaterials* **2000**, *21*, 2067.
(20) Bernkop-Schnürch, A. *Int. J. Pharm.* **2000**, *194*, 1.
(21) Lorenzo-Lamosa, M. L.; Remunan-Lopez, C.; Vila-Jato, J. L.; Alonso, M. J. *J. Controlled Release* **1998**, *52*, 109.
(22) Amornchai, W.; Hoven, V. P.; Tangpasuthadol, V. *Macromol. Symp.* **2004**, *216*, 99.
(23) Borges, O.; Borchard, G.; Coos Verhoef, J.; de Sousa, A.; Junginger, H. E. *Int. J. Pharm.* **2005**, *299*, 155.
(24) Juang, R. S.; Wu, F. C.; Tseng, R. L. *Adv. Environ. Res.* **2002**, *6*, 171.
(25) Durán, N.; Rosa, M. A.; D'Annibale, A.; Gianfreda, L. *Enzyme Microb. Technol.* **2002**, *31*, 907.
(26) Chiou, S. H.; Wu, W. T. *Biomaterials* **2004**, *25*, 197.
(27) Juang, R. S.; Wu, F. C.; Tseng, R. L. *Bioresour. Technol.* **2001**, *80*, 187.
(28) Peniche, H.; Osorio, A.; Acosta, N.; de la Campa, A.; Peniche, C. *J. Appl. Polym. Sci.* **2005**, *98*, 651.
(29) le Dung, P.; Milas, M.; Rinaudo, M.; Desbrieres, J. *Carbohydr. Polym.* **1994**, *24*, 209.
(30) Sieval, A. B.; Thanou, M.; Kotzé, A. F.; Verhoef, J. C.; Brussee, J.; Junginger, H. E. *Carbohydr. Polym.* **1998**, *36*, 157.
(31) Kim, C. H.; Choi, J. W.; Chun, H. J.; Chio, K. S. *Polym. Bull.* **1997**, *38*, 387.
(32) Shi, Z.; Neoh, K. G.; Kang, E. T.; Wang, W. *Biomaterials* **2006**, *27*, 2440.
(33) Singla, A. K.; Charla, M. J. *J. Pharm. Pharmacol.* **2001**, *53*, 1047.
(34) Thanou, M. M.; Kotzé, A. F.; Scharringhausen, T.; Lueben, H. L.; de Boer, A. G.; Verhoef, J. C.; Junginger, H. E. *J. Controlled Release* **2000**, *64*, 15.
(35) Kotzé, A. F.; Lueβen, H. L.; de Leeuw, B. J.; de Boer(A)B. G.; Verhoef, J. C.; Junginger, H. E. *Pharm. Res.* **1997**, *14*, 1197.
(36) Thanou, M.; Florea, B. I.; Langemeÿer, M. W. E.; Verhoef, J. C.; Junginger, H. E. *Pharm. Res.* **2000**, *17*, 27.
(37) Jonker, C.; Hamman, J. H.; Kotzé, A. F. *Int. J. Pharm.* **2002**, *238*, 205.
(38) Kotzé, A. F.; Lueβen, H. L.; de Leeuw, B. J.d; de Boer(A)B. G.; Verhoef, J. C.; Junginger, H. E *J. Controlled Release* **1998**, *51*, 35.
(39) Cano-Cebrián, M. J.; Zornoza, T.; Granero, L.; Polache, A. *Curr. Drug Del.* **2005**, *2*, 9.
(40) Chang, Y. C.; Shieh, D. B.; Chang, C. H.; Chen, D. H. *J. Biomed. Nanotech.* **2005**, *1*, 196.
(41) Jiang, D. S.; Long, S. Y.; Huang, J.; Xiao, H. Y.; Zhou, J. Y. *Biochem. Eng. J.* **2005**, *25*, 15.
(42) Park, J. H.; Im, K. H.; Lee, S. H.; Kim, D. H.; Lee, D. Y.; Lee, Y. K.; Kim, K. M.; Kim, K. N. *J. Magn. Magn. Mater.* **2005**, *293*, 328.
(43) Hu, Q.; Chen, F.; Li, B.; Shen, J. *Mater. Lett.* **2006**, *60*, 368.
(44) Denkbas, E. B.; Kilicay, E.; Birlikseven, C.; Ozturk, E. *React. Funct. Polym.* **2002**, *50*, 225.
(45) Lee, H. S.; Kim, E. H.; Shao, H.; Kwak, B. K. *J. Magn. Magn. Mater.* **2005**, *293*, 102.
(46) An, X.; Su, Z. *J. Appl. Polym. Sci.* **2001**, *81*, 1175.
(47) An, X.; Su, Z. J.; Zeng, H *J. Chem. Technol. Biotechnol.* **2003**, *78*, 596.

min), washed twice with deionized water and air-dried by spreading on a glass plate.

Preparation of Magnetic Chitosan Nanoparticles. A 1% (w/v) chitosan stock solution was prepared by dissolving 1 g of chitosan in 100 mL of 2% (v/v) acetic acid solution followed by a 5 h sonication to dissolve the chitosan completely. Magnetic chitosan nanoparticles were obtained from the dispersion of freshly precipitated, not dried magnetite, in the above 1% (w/v) chitosan solution (pH ~ 3.5, zeta potential = +48 mV, size = 3700 nm).

Three samples with a weight ratio of $m_{chitosan}/m_{Fe_3O_4} = 1$, 2, and 4 were prepared by dispersing the magnetite pulp from the above preparation, i.e. ~ 390 mg, into 39, 78, and 117 mL of 1% (w/v) chitosan solution. In each case, the magnetic−chitosan mixture was diluted to 150 mL, stirred for 1 h at room temperature and then the acidic solution was neutralized with a 10% (w/v) solution of $NaHCO_3$. After the foam was subsided, the precipitate was collected by centrifugation, washed twice with deionized water and spread on a glass plate for drying. The film formed was transferred to 50 mL of water and then acidified to pH 2.7 with a 2% (w/v) solution of acidic acid. A hydrosol was formed which was centrifuged at 1000 rpm for 2 min and the supernatant was collected. Addition of alcohol caused precipitation of the magnetic chitosan, which was isolated by centrifugation, washed with alcohol and dried in air. The final material is readily soluble in water (20 mg/mL) giving a pH 2.8. The samples are denoted by C1F1, C2F1, and C4F1.

Preparation of Magnetic−NQC Nanoparticles. Highly substituted *N*-trimethyl chitosan (pH ~ 4.4−5.7, $z = +38$ mV, $s = 500$ nm) was synthesized following the two-step synthesis described by Sieval.[30] Magnetite was prepared as above but it was acid peptized at pH ~ 3 before dispersion. Derivatives of magnetite with quaternized chitosan (MNQC) with a weight ratio of $m_{NQC}/m_{Fe_3O_4} = 1$ were obtained by dispersion of the magnetite pulp from the above-mentioned preparation in a 1% (w/v) NQC solution. The magnetite−NQC derivative was isolated as in the case of magnetite−chitosan samples. The MNQC ferrofluids had a concentration of 20 mg/mL.

Characterization. X-ray powder diffraction (XRD) patterns were taken on a D-500 Siemens diffractometer using Cu Kα radiation ($\lambda = 1.5418$ Å). Thermogravimetric (TG) analysis and differential thermal analysis (DTA) were made in an air atmosphere between 25 and 1000 °C using a TGA/DTA 6200 Exstar thermal analyzer (Seiko Instruments, Inc.) with a sample weight of 7−10 mg and thermal gradient of 5 °C/min. FT-IR spectra were collected on a Bruker, Equinox 55/S model in the region of 400−4000 cm^{-1} with 32 successive scans. The samples were measured in the form of KBr pellets (Aldrich, 99%, FT-IR grade). Zeta-potential measurements were carried out with a Zeta Sizer instrument (Malvern Instruments) using the electrophoresis method. The measurements based on electrophoretic mobility of the nanoparticles in diluted aqueous suspensions were performed at least for triplicate with independent particle batches. Mössbauer spectra were recorded between 25 and 300 K in a constant acceleration mode with a 50 mCi $^{57}Co(Rh)$ source moving at room temperature, while the sample was placed in a variable temperature cryostat. Isomer shift values are reported with respect to α-Fe. External magnetic field Mössbauer measurements were performed at 5 K in a field of 5 T applied parallel to the gamma-ray direction (Oxford Instruments). Particle size and morphology of magnetic chitosan nanoparticles were evaluated from TEM micrographs using a JEM2010 microscope operated at 200 kV and characterized by a point-to-point resolution of 1.9 Å. Before measurements, the samples were dispersed in ethanol and the suspension was treated in ultrasound for 10 min. A drop of very dilute suspension was placed on a carbon-coated grid and allowed to dry by evaporation at ambient temperature. A superconducting quantum interference device (SQUID, MPMS XL-7, Quantum Design) was used for the magnetic measurements. The hysteresis loops were recorded at 2 and 298 K in external magnetic fields up to 5 T.

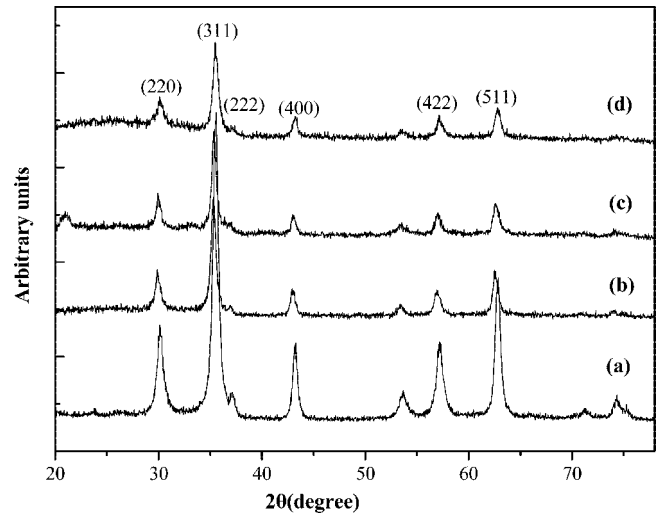

Figure 1. XRD pattern of the (a) magnetic quaternized chitosan and of the magnetic chitosan composites (b) C1F1, (c) C2F1, and (d) C4F1.

Results and Discussion

Preparation, Properties, and Characterization of Magnetic−Chitosan Hybrids. Stable hydrosols of a magnetic iron oxide were obtained by dispersing a freshly prepared pulp of the oxide in a chitosan solution. The resulting magnetic oxide−chitosan derivatives are positively charged from the protonation of the amine groups and thus are present in the form of a hydrosol. Neutralization with $NaHCO_3$ causes precipitation enabling further isolation of the magnetic chitosan. This product is easily dispersed in acidic solution from which is isolated by addition of alcohol. This procedure provided ferrofluids with high concentrations of magnetic oxide (20 mg/mL) that were stable for more than 3 weeks without signs of solid precipitation. Longer retention times caused a cloudy appearance and finally after 1 month a solid precipitate was settled out.

The XRD patterns of the C1F1, C2F1, C4F1, and MNQC magnetic hybrids (see Figure 1) show characteristic 2θ reflections at 30.1 (220), 35.5 (311), 37.2 (222), 43.1 (400), 53.4 (422), 57.0 (511), and 62.6 (440) that indicate formation of a nanocrystalline spinel phase from either Fe_3O_4 or γ-Fe_2O_3 with an average size, between 14−18 nm as estimated from the Scherrer equation. Since the oxides are isostructural and, moreover, exist in nanophase state their XRD identification is difficult. The Mössbauer results that follow discern the two oxides and recognize the formation of nonstoichiometric magnetite.

In the three derivatives, the extent of the oxide surface coating ranged between 7 and 10 wt % as derived from TG analysis, all after the subtraction of the adsorbed water. These values indicate a low content of the organic phase, although it covers fully the magnetic cores as will be discussed below with the representative sample C4F1. Due to the low percentage of the chitosan shell, the system reveals a high

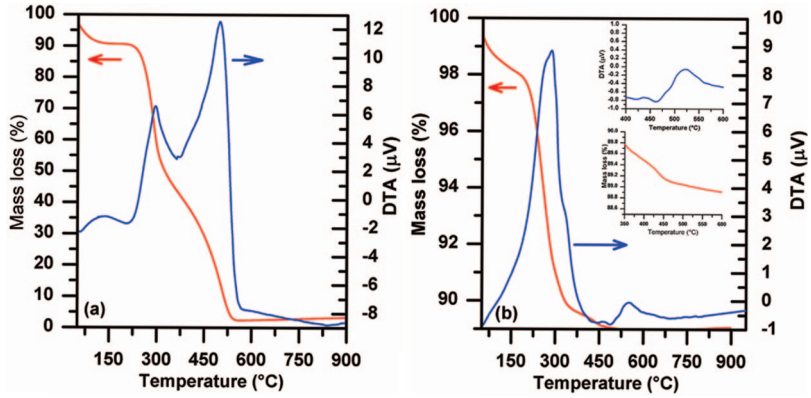

Figure 2. TG-DTA curves of the free chitosan (left) and the C4F1 sample (right), recorded in air at 5 °C/min.

saturation magnetization, a property highly desired for biomedical applications.

To consider the thermal stability of the prepared magnetite−chitosan hybrids and to understand the nature of an interaction of the magnetic core with the organic shell, we measured the simultaneous TG/DTA curves of the C4F1 sample and, for comparison, of the pure free chitosan (see Figure 2). The TG/DTA analysis of the free chitosan indicates two-step decomposition process in air with well separated steps and maxima at ca. 300 and 500 °C. The decomposition process is completed at ca. 550 °C. The analysis of the magnetite−chitosan hybrid at the same heating conditions shows that the decomposition process is almost completed around 350 °C, although, it has also two step response with the strongly overlapped exothermic processes taking place in the temperature range of 200−350 °C (see Figure 2, right). This difference in the thermal stability of magnetite−chitosan hybrid is probably due to the narrow nanoscopic shell of chitosan attached to the surface of the magnetic core in the framework of the hybrid structure compared to the free chitosan with a well-developed polymeric structure. The exoeffect observed around 525 °C in the DTA curve (see Figure 2 right including a top inset) can be clearly attributed to the transformation of the magnetic phase to hematite as confirmed by XRD measurement of the C4F1 sample (not shown) heated in dynamic conditions of thermal analysis up to 525 °C, where a mixture of maghemite-(magnetite) and hematite was identified. These thermal results demonstrate that chitosan capping improves the thermal stability of the magnetic phase. In order to clarify definitely the improved thermal stability of magnetic cores caused by the chitosan coating, we analyzed the C4F1 sample heated in dynamic conditions of the DTA analysis up to 460 °C (after the first intense exoeffect). Indeed both XRD and Mössbauer data (not shown) unambiguously proved the presence of the only nonstoichiometric maghemite (magnetite) without traces of hematite.

The FT-IR spectra of the magnetite, magnetic chitosan C4F1 and magnetic quaternized chitosan (MNQC) derivatives are shown in Figure 3. The spectra clearly indicate the presence of chitosan and quaternized chitosan in the hybrid samples. Thus, the broad peak at 3422 cm^{-1} arises from the combined O−H stretching and intermolecular hydrogen bonding vibrations. The vibrations of the N−H stretching from primary amines are masked in the same region. The

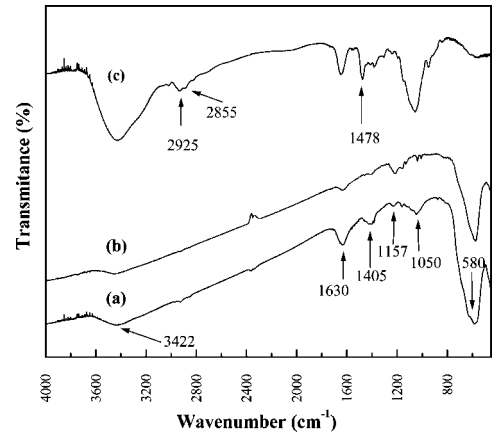

Figure 3. FT-IR spectra of (a) C4F1, (b) Fe_3O_4, and (c) magnetic quaternized chitosan.

C−H stretching vibrations of the polymer are clearly seen at 2925 cm^{-1} and 2855 cm^{-1} for the MNQC sample. The absorption near 1630 cm^{-1} comes from the C═O amide stretching and that at 1405 cm^{-1} from the N−H stretching of the amide. The C−O−C stretching vibration occurs near 1050 cm^{-1}, while the quaternized derivative shows a vibration at 1478 cm^{-1} from the quaternized ammonium structure at the C-2 position in the chitosan.[32] Finally, all spectra show a broad absorption centered at 580 cm^{-1} indicating formation of the iron oxide framework.

The pH and zeta potential (z) were found to be 3.5 and +47.7 ± 3.6 for free chitosan, 4.4 and +47.7 ± 4.2 for quaternized chitosan, 4.7 and +33.2 ± 4.5 for magnetic composite C1F1, 4.7 and +38.6 ± 5.6 for magnetic composite C2F1, 4.6 and +37.9 ± 8.3 for magnetic composite C4F1, and 4.7 and 38 ± 0.5 for MNQC sample. The comparable pH and z values of the different magnetite−chitosan derivatives suggest similar chitosan coating on the oxide surfaces. Furthermore, as the magnitude of zeta potential is generally accepted as a marker for the stability of colloidal systems, the observed high zeta potential values, explain the stability of the particle suspensions in water.

TEM Characterization. TEM micrographs exhibit well defined particles sized between 20 and 40 nm, mainly of cubic morphology embedded in the chitosan matrix (see Figure 4). The successful capping is clearly seen in Figure 5, where the narrow organic shells are indicated by arrows.

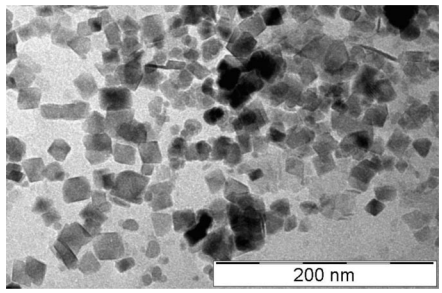

Figure 4. TEM micrograph of iron oxide nanoparticles embedded in the chitosan matrix.

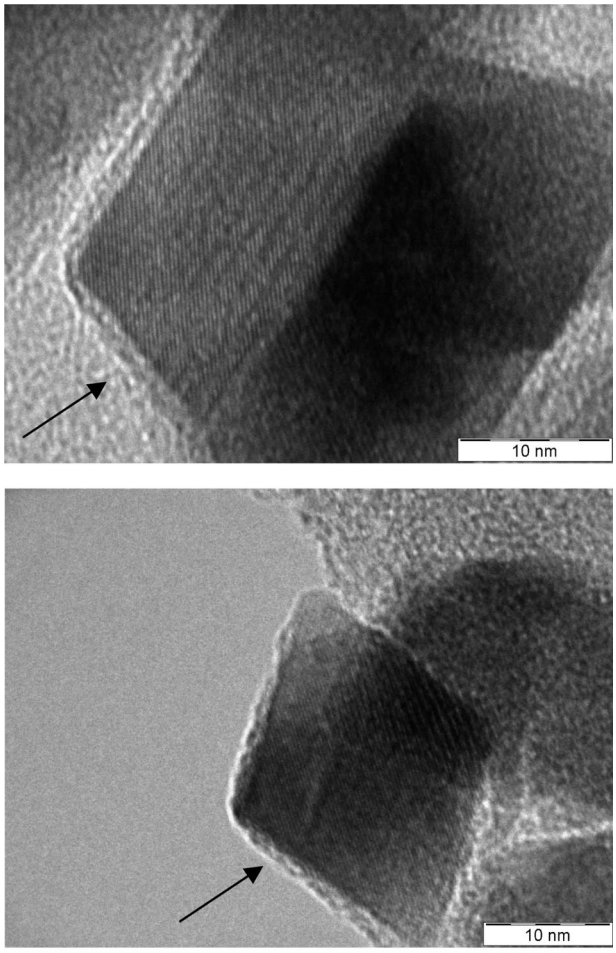

Figure 5. TEM micrographs demonstrating well developed cubic nanocrystallites of magnetite capped with the chitosan shell.

Mössbauer Analysis. Mössbauer spectra, particularly obtained in presence of an externally applied magnetic field and at low temperatures, comprise a powerful tool for structural and magnetic characterization of iron oxides. Magnetite and maghemite, both having a spinel structure, can be easily identified and distinguished on account of the divalent iron present in the octahedral sites of magnetite. Thus, the iron atoms in octahedral positions of the magnetite structure have an isomer shift (δ) value near 0.67 mm/s at room temperature which lies between those of Fe(III) and Fe(II) because of electron delocalization on these sites. However, this value decreases significantly if the Fe(III) atoms prevail in octahedral positions, as in the case of nonstoichiometric magnetite samples.

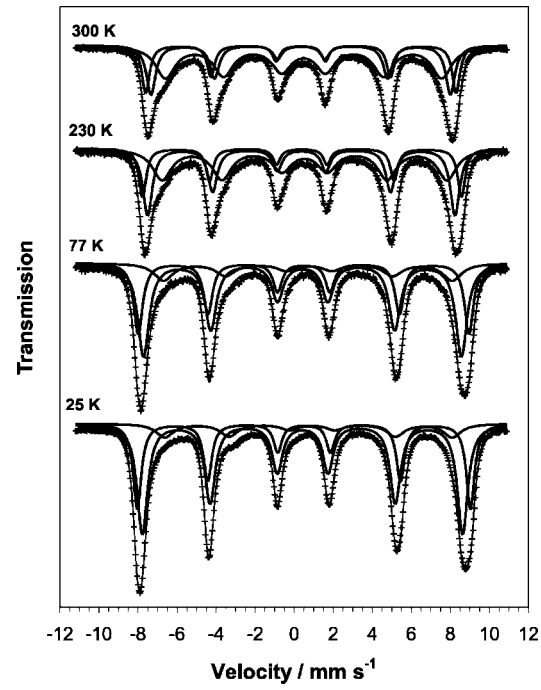

Figure 6. Temperature dependent Mössbauer spectra of the C4F1 sample.

The spectra of the C4F1 sample measured at different temperatures (25−300 K) are shown in Figure 6, and the derived hyperfine parameters are listed in Table 1.

The first important observation is the lack of a superparamagnetic doublet in room temperature spectrum, meaning that the particles are large enough and thus their magnetic moment is blocked within the time window ($\sim 10^{-8}$ s) of the Mössbauer experiment. The fact that the same sample exhibits a superparamagnetic behavior at 300 K in magnetic measurements (see magnetic measurements) arises from the different time scale of the technique ($\sim 10^{2}$ s).

The spectra were fitted with three magnetically split sextets that differ in their hyperfine parameters. Two sextets are ascribed to Fe(III) centers and the third one with a higher δ (0.51 mm/s at room temperature) represents the fraction of iron atoms with an intermediate valence state Fe(II−III). Regarding the Fe(III) sextets, the narrower sextet with larger hyperfine magnetic field is attributed to the iron atoms in the interior of the crystallites, while the other broader Fe(III) sextet, which narrows progressively and increases in hyperfine field with decreasing temperature, arises probably from the surface iron atoms. Finally, the third sextet, assigned to an intermediate iron valence state, has isomer shift values that increase progressively with lowering temperature (0.80 mm/s at 25 K), and at the same time, its spectral area decreases drastically. Such a behavior indicates that the fraction of Fe(II) atoms in the structure becomes more and more resolved and separated from the Fe(III) atoms in the low temperature spectra. The spectral area of this sextet is 10% at 25 K, which is the same as the percentage of divalent iron determined from in-field Mössbauer measurements that follow. We thus conclude that the main results from the temperature dependent Mössbauer spectra are the lack of superparamagnetic doublet in the RT spectrum, being in accordance with the dimensions of crystallites found from

Table 1. Mössbauer Parameters of the C4F1 Sample Measured at Temperatures 300−25 K[a]

T [K]	component	$\delta \pm 0.01$ [mm/s]	$\varepsilon_Q \pm 0.01$ [mm/s]	$B_{hf} \pm 0.5$ [T]	RA ± 1 [%]	assignment
300	sextet 1	0.33	0.01	49.4	19	Fe^{3+}
	sextet 2	0.34	− 0.01	47.6	29	Fe^{3+}
	sextet 3	0.48	− 0.01	44.0	52	Fe^{3+}+ Fe^{2+}
230	sextet 1	0.38	0.01	50.7	19	Fe^{3+}
	sextet 2	0.36	0.00	48.9	36	Fe^{3+}
	sextet 3	0.53	−0.02	45.4	45	Fe^{3+} + Fe^{2+}
77	sextet 1	0.48	0.01	52.7	29	Fe^{3+}
	sextet 2	0.43	0.00	50.6	53	Fe^{3+}
	sextet 3	0.72	−0.06	46.2	18	Fe^{3+} + Fe^{2+}
25	sextet 1	0.50	−0.01	53.0	33	Fe^{3+}
	sextet 2	0.45	0.02	51.0	57	Fe^{3+}
	sextet 3	0.80	−0.10	46.0	10	Fe^{2+}

[a] T = temperature of measurement, δ = isomer shift (related to metallic iron), ε_Q = quadrupole shift, B_{hf} = hyperfine magnetic field, RA = relative spectrum area.

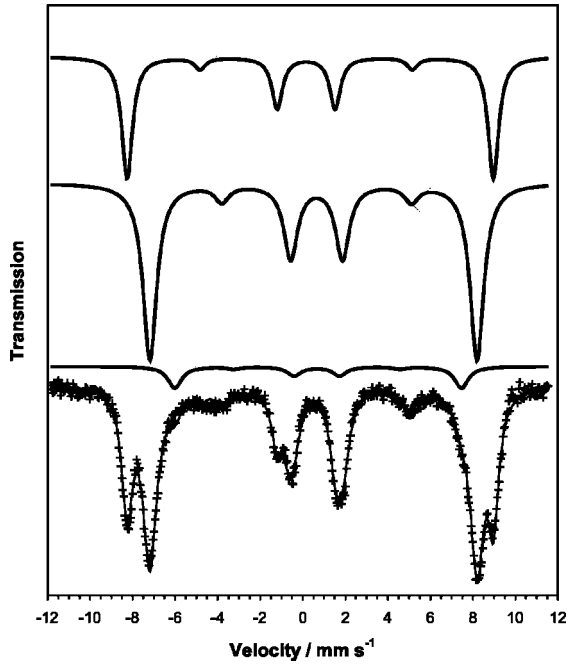

Figure 7. Mössbauer spectrum of C4F1 sample measured at 5 K in external field of 5 T, applied parallel to the gamma-ray direction.

TEM, and the presence of a fraction of 10% of Fe(II) atoms implying the formation of "nonstoichiometric magnetite". Taking into account the found content of Fe(II) atoms, the stoichiometry of the magnetic particles can be expresses by the formula of $Fe^{III}_{1.90}Fe^{II}_{0.10}O_{2.95}$.

To further study the structural and magnetic ordering of iron oxide nanoparticles, Mössbauer spectra were recorded for the sample C4F1 at 5 K in an external magnetic field of 5 T applied parallel to the gamma ray direction (see Figure 7). The results of the fitting procedure, including the hyperfine parameters, are summarized in Table 2. The spectrum can be well fitted with three sextets differing mainly in the values of the isomer shift and effective magnetic field. Two of the magnetically split components with the isomer shift values of 0.28 and 0.59 mm/s could be well ascribed to Fe(III) in the tetrahedral A and octahedral B positions in a potential maghemite structure.

However, the isomer shift corresponding to octahedral B site is slightly higher than that reported for pure nanosized maghemite.[48] This reflects the possible involvement of divalent iron in the octahedral B positions. The third low-field sextet with the highest isomer shift, typical of divalent iron (0.74 mm/s), offers substantial support to the assumption that the magnetic particles can be assigned to "nonstoichiometric magnetite". The nonzero quadrupole shift parameters found for all three sextets are also characteristic for (nonstoichiometric) magnetite below the Verwey transition temperature,[49] while maghemite usually yields values close to zero.

From the application viewpoint, we must indicate that independently of the nonstoichiometry in the magnetite structure the particles exhibit very good crystallinity and well defined cubic shape, as confirmed by TEM analysis, along with the perfect ferrimagnetic ordering with a low degree of spin canting and frustration. The latter can be deduced from the very low intensities of the second and the fifth lines in the in-field Mössbauer spectrum, which provide evidence for the perfect ordering of atomic moments in the external magnetic field. Furthermore, these lines are also reduced in the case of the Fe(II) component indicating that this is not an impurity or a separate phase, but that Fe(II) cations participate in the spinel structure.

Magnetic Measurements. The magnetization vs applied field curves of the representative C4F1 sample were measured at temperatures of 2 and 298 K (see Figure 8). The room temperature curve is typical of superparamagnetic particles exhibiting no hysteresis above their blocking temperature. As the temperature decreases, the magnetic moment of the particles become progressively blocked in the time scale of the magnetic measurements, showing a kind of ordered state from the assembly of magnetic hybrid particles. At 2 K, the sample displays a weak hysteresis loop typical of nanocrystalline magnetite. After subtraction of the chitosan content, the saturation magnetization at 2 K for the magnetic oxide (∼80 emu/g) is very high among such nanocrystalline systems and is close to the value of 90 emu/g reported for bulk magnetite.[50] Similarly to the saturation magnetization, the coercive field H_C of 180 Oe is only slightly lower than for bulk magnetite. Analogous decrease in the hysteresis parameters has been observed for magnetic iron oxide nanosystems and attributed to the small size of

(48) Tucek, J.; Zboril, R.; Petridis, D. *J. Nanosci. Nanotechnol.* **2006**, *6*, 926.
(49) Doriguetto, A. C.; Fernandes, N. G.; Persiano, A. I. C.; Nunes Filho, E.; Grenèche, J M.; Fabris, J. D. *Phys. Chem. Miner.* **2003**, *30*, 249.
(50) Schneeweiss, O.; Zboril, R.; Pizurova, N.; Mashlan, M.; Petrovsky, E.; Tucek, J. *Nanotechnology* **2006**, *17*, 607.

Table 2. Mössbauer Parameters of the C4F1 Sample at 5 K in an External Field of 5 T[a]

component	$\delta \pm 0.01$ [mm/s]	$\varepsilon_Q \pm 0.01$ [mm/s]	$B_{eff} \pm 0.5$ [T]	RA $\pm$ 1 [%]	assignment
sextet I	0.28	0.18	53.5	32	Fe^{3+}−tetrahedral A
sextet II	0.59	− 0.14	47.8	58	Fe^{3+}−octahedral B
sextet III	0.74	0.10	41.8	10	Fe^{2+}−octahedral B

[a] δ = isomer shift (related to metallic iron), ε_Q = quadrupole shift, B_{eff} = effective hyperfine magnetic field, RA = relative spectrum area.

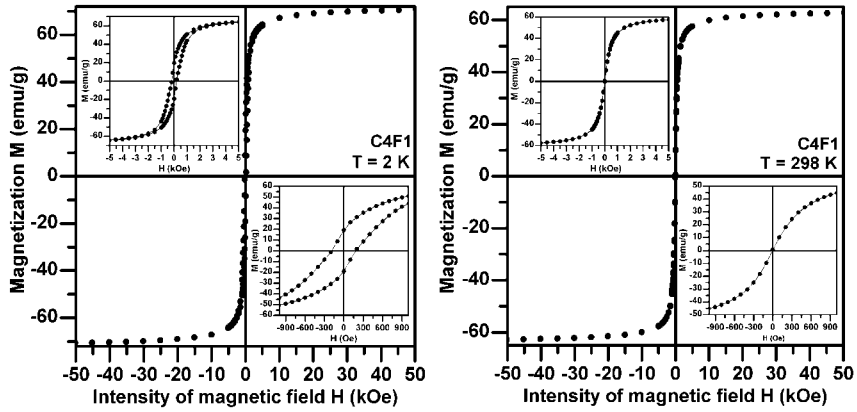

Figure 8. Hysteresis loops of C4F1 sample, measured at temperatures of 2 (left) and 298 K (right).

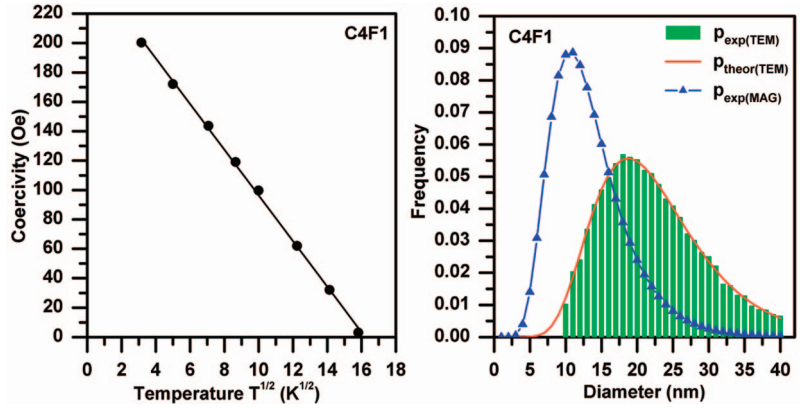

Figure 9. Coercive field versus temperature (left) and comparison of the particle size distribution determined from TEM with the magnetic size calculated from the field dependence of the magnetization at 298 K (right). The solid line represents the theoretical curve assuming the log-normal size distribution.

the particles and the presence of a magnetically inactive coating (i.e., chitosan) on the surface of the nanoparticles.

As clearly seen in Figure 8, the room temperature hysteresis loop already saturates at low applied magnetic fields (1−1.5 T). This behavior together with negligible intensities of the second and the fifth line in the in-field Mössbauer spectrum confirm that the synthesized particles do not possess any significant surface spin canting and disorder and therefore negligible broken bonds for frustration of the antiferromagnetic exchange interactions between the magnetically active Fe^{3+} ions in the magnetic unit. In addition, on account of the easily saturated hysteresis loops at low applied magnetic fields, the strength of interparticle interactions among the particles is reduced through the coating of their surfaces with chitosan. The successful coating of particles, proved by TEM and thermal analysis, is further documented from the measurements of the temperature dependence of the coercivity below the blocking temperature T_B. The recorded linear dependence of H_C on $T^{1/2}$ (see Figure 9, left), following the equation $H_C(T) = H_C(0)(1 - (T/T_B)^{1/2})$, reflects the behavior of a system of noninteracting (i.e., well capped) single-domain particles.[51] From Figure 9, one can derive a temperature at which the coercivity of the system drops to zero. As the system exhibits a size distribution, this temperature (~250 K) can be assigned to the blocking temperature of the largest particles.

In order to get deeper insight into the properties of C4F1 sample, the estimation of the magnetic size of the particles (i.e., the size of the magnetite core) was calculated by employing the Chantrell model[52] and assuming noninteracting superparamagnetic particles with a log-normal size distribution (see Figure 9, right). These calculations lead to a mean size value of 14 nm for the magnetic core, which is in good accordance with the mean size of the composite particles observed from TEM (20 nm) and exhibiting a log-normal size distribution (see Figure 9, right). Taking into account the symmetric particle shape, the difference between

(51) Cullity, B. D. *Introduction to magnetic materials*; Addison-Wesley: Reading, MA, 1972.
(52) Chantrell, R. W.; Popplewell, J.; Charles, R. W. *IEEE Trans. Magn.* **1978**, *14*, 975.

the mean sizes of the magnetic core and the coated particles we conclude that the thickness of the chitosan shell is about 4 nm, in good agreement with the high resolution TEM images (see Figure 5). Since the model supposes an assembly of noninteracting particles, within the experimental errors of the measuring techniques, the observed good concordance between the results from TEM and magnetic measurements represents another evidence of the successful capping of the magnetic oxide framework through a chitosan shell. To evaluate further the presence of interparticle interactions, reduced remanence M_R/M_S has been calculated. Recently, the theoretical M_R/M_S value of 0.5 at 0 K has been experimentally reported for an assembly of noninteracting single domain particles of various systems.[53] The extrapolated value of $M_R/M_S = 0.42$ for C4F1 sample is slighty lower than the theoretical, supporting the very low degree of interparticle interactions taking into account the powdered character of the sample. However, this ratio is much higher than that reported for strongly interacting magnetite nanoparticles,[54] suggesting that the inteparticle interactions in the present case are rather negligible. Summarizing, the observed room temperature superparamagnetic behavior of the coated magnetite nanocomposite, the high saturation magnetization reached at relatively low applied fields (≈1.5 T), the suppressed interparticle interactions and the low degree of particle agglomeration make the present biocompatible magnetic complexes promising agents for use in practical applications where strong magnetic signal at small applied magnetic fields is required (e.g., MRI, magnetic separation techniques, drug delivery, etc.).

(53) Tung, L. D.; Kolesnochenko, V.; Caruntu, D.; Chou, N. H.; O'Connor, J.; Spinu, L *J. Appl. Phys.* **2003**, *93*, 7486.
(54) Goya, G. F.; Berquó, T. S.; Fonseca, F. C.; Morales, M. P. *J. Appl. Phys.* **2003**, *94*, 3520.

Conclusions

We have described the preparation of magnetic nanocomposites made up of nonstoichiometric magnetite as a core and chitosan as a biocompatible shell. Such a system has a high application potential in biomedicine due to the suitable biochemical properties of the chitosan shell in conjunction with a set of superior physicochemical characteristics of the composite including the following:

- sufficient stability;
- very high saturation magnetization reachable at low applied field;
- superparamagnetic behavior at room temperature;
- perfect ferrimagnetic ordering with a low degree of spin frustration bellow the blocking temperature (and/or in the external magnetic field);
- low content of organic matrix;
- capping of the magnetic core with the chitosan shell preventing the particle agglomeration;
- well defined cubic shape particles with a size range (10−40 nm) suitable for biomedical applications.

Acknowledgment. This work has supported by the Projects of the Ministry of Education of the Czech Republic (1M619895201 and MSM6198959218) and by the project of ACSR (KAN115600801).

CM702990T